Submicrometer control of two-dimensional–two-dimensional magnetotunneling in double-well heterostructures

J. A. Simmons, S. K. Lyo, J. F. Klem, M. E. Sherwin, and J. R. Wendt
Sandia National Laboratories, Albuquerque, New Mexico 87185
(Received 21 January 1993)

Interwell two-dimensional–two-dimensional (2D-2D) tunneling in a density-imbalanced double-well heterostructure is studied in an in-plane magnetic field using a gated-bridge technique which does not require independent contacts to the two 2D electron layers. Two sharp peaks in the tunneling conductance at $B \leq 1.3$ T and $B = 5$–6 T are explained using a linear-response theory which incorporates finite scattering and is based on a field-induced momentum shift of the two quantum wells' Fermi circles. A second gate is used to locally enhance tunneling on a submicrometer length scale.

The past several years have seen tremendous interest in double-barrier resonant-tunneling devices in which the tunneling is from three-dimensional (3D) to two-dimensional (2D).[1] In the presence of an in-plane magnetic field B, the resonant-tunneling $I(V)$ peak undergoes a voltage shift and considerable broadening.[2–5] Zaslavsky *et al.*[5] proposed a geometrical construction, in which the dispersion curves for the 3D emitter and 2D quantum well (QW) are plotted in (k_x, k_y, E) space, with their origins offset by a B-induced shift in transverse momentum Δk. Requiring conservation of energy and transverse momentum, the tunneling is possible only when the dispersion curves overlap.

More recently, 2D–2D tunneling has become of interest. Smoliner *et al.*[6] examined nonequilibrium (i.e., at bias voltages $\gg kT$) magnetotunneling between an accumulation and an inversion layer. Eisenstein *et al.*[7] examined equilibrium magnetotunneling in a double-QW system with initially balanced electron densities, as a function of both B and the QW's density ratio. A similar geometrical model, modified to the equilibrium 2D-2D case, was used to explain their results. In these works, the two 2D electron layers were contacted independently, either using diffused contacts,[6] or by thinning the sample and patterning both sides with gates.[7,8]

In this work, we report on our studies of equilibrium 2D-2D magnetotunneling in a double-QW GaAs heterostructure with a built-in density imbalance. We avoid the difficult task of contacting the two electron layers independently by using a gate to deplete the top QW across a small region of a resistance bridge, and then measuring the four-terminal source-drain resistance $R_{SD}(B)$. We establish a formal relationship between $R_{SD}(B)$ and the tunneling conductance $G_{tun}(B)$ in terms of a transmission-line model. $G_{tun}(B)$ is then obtained from the measured $R_{SD}(B)$. Two sharp peaks are observed in $G_{tun}(B)$ and explained in terms of the two QW's B-displaced Fermi circles intersecting one another tangentially.[7] We present a linear-response theory, incorporating finite scattering times, which shows good agreement with the data. Finally, we use a second 0.3-μm-wide gate to locally control tunneling on a submicrometer length scale.

Our sample is a molecular-beam-epitaxy (MBE) -grown heterostructure consisting of two 150-Å GaAs wells separated by a 65-Å $Al_{0.3}Ga_{0.7}As$ barrier. A 7×10^{11} cm^{-2} Si δ-doped layer lies 800 Å beneath the bottom well (QW1), while a 250-Å-wide 10^{18} cm^{-3} Si-doped region is 450 Å above the top well (QW2). When cooled to 0.3 K in the dark, QW1 typically has density $n_1 = 1.8\times10^{11}$ cm^{-2} and mobility 6×10^4 $cm^2/V\,s$, while QW2 typically has density $n_2 = 1.0\times10^{11}$ cm^{-2} and mobility 6×10^5 $cm^2/V\,s$, as determined by Shubnikov–de Haas measurements. (These density values can vary by $\sim10\%$ on thermal cycling, and the mobility values by as much as 50%.) Using electron-beam lithography, the sample is patterned into a bridge geometry of 15-μm length and 2-μm width. Two 0.3-μm-wide Cr/Au gates are placed across the bridge, somewhat off center, and separated from each other by 2 μm center to center (see Fig. 1). R_{SD} is measured using a standard 17-Hz lock-in technique at 0.3 K for $B \leq 14$ T applied parallel to the growth plane. Excitation voltages are ≤ 100 μV, much smaller than the electrons' Fermi energies of ~5 meV.

Shown in Fig. 2 is R_{SD} as a function of the voltage V_A on gate A, for $B = 0$, and gate B at voltage $V_B = 0$. At $V_A = 0$, both wells carry current, and R_{SD} is largely determined by QW2, which has much higher conductivity. As V_A is biased, R_{SD} increases from ~1.3 kΩ until a plateau at ~10 kΩ is reached at $V_A = V_{depl} = -0.42$ V, when QW2 is depleted. R_{SD} thus increases by a factor of ~7, even though the effective gate width is $\leq 1/10$th of the length of the channel. This is because at $B = 0$ the tunneling resistance is very high, and once the QW2 current channel is broken, the current must largely flow in QW1. Increasing V_A further also depletes QW1, eventually pinching it off at $V_A = -0.6$ V.

The suppressed tunneling at $B = 0$ can be understood[6,7] by assuming the electrons to be localized in QW1 or QW2. The dispersion curve of the system then has two branches, one for each QW, identical except for an energy offset. Only those pairs of states with identical momentum, one in each QW, and both at the Fermi surface, can participate in tunneling. Since the densities of the two wells are substantially different, their Fermi cir-

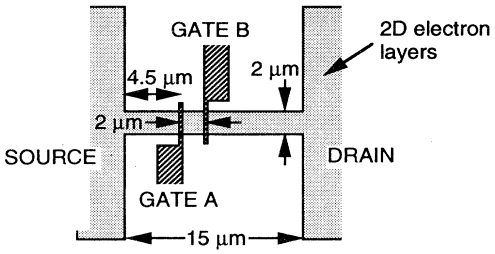

FIG. 1. The diagram of the sample. Shaded regions represent 2D electron layers, and hatched regions 0.3-μm-wide gates.

cles are located concentrically in momentum space with no overlap, and no interwell pairs of states having the same momentum and energy exist.

Before examining the model at finite B, we discuss the equivalent circuit used to obtain the tunneling resistance from the measured R_{SD}. In the upper-left inset to Fig. 2 is pictured schematically the situation when $V_A = V_{depl}$ and $V_B = 0$. (Because QW2 has much higher conductivity than QW1, the tunneling current increases toward the edges of gate A; other current paths offer higher resistance.) In the lower-left inset, a transmission-line model[9] equivalent circuit for the region of the sample to the right of gate A is shown. Using the boundary conditions that the top and bottom well voltages are equal to one another at the source and drain, and that the top well current is zero under the gate, we obtain, for the resistance of the right region,

$$R_{\text{right}} = \frac{R_{BR}^2}{R_{BR}+R_{TR}} \frac{\tanh\beta_R}{\beta_R} + \frac{R_{BR}R_{TR}}{R_{BR}+R_{TR}}, \qquad (1)$$

where $\beta_R^2 = (R_{BR}+R_{TR})/R_{\text{tun}R}$. Here R_{BR} and R_{TR} are the resistances of the right-hand sides of the bottom and top QW's, and $R_{\text{tun}R}$ is the net tunneling resistance between the wells on the right side of the gate. Thus R_{right} varies between R_{BR}, when $R_{\text{tun}R} = \infty$, and $(1/R_{TR} + 1/R_{BR})^{-1}$, when $R_{\text{tun}R} = 0$. The left-side resistance R_{left} is obtained in a similar manner. [Numerical simulations reveal that, because the left side is less than half as long as the right, and because of the way β scales with length, and the general nonlinear nature of the circuit, the magnetoresistance (MR) appears mostly through R_{right}.] Thus $R_{SD} = R_{\text{right}} + R_{\text{left}} + R_{BG}$, where R_{BG} is the resistance of that portion of the bottom well under the gate. If the R_T's and R_B's are independent of B, $R_{SD}(B)$ then becomes a good measure of the magnetotunneling. That this is the case is shown in the upper-right inset to Fig. 2, where $R_{SD}(B)$ is shown for $V_B = 0$ and several values of V_A. When $V_A = 0$, so that $R_{SD} = [1/(R_{TL}+R_{TR}+R_{TG}) + 1/(R_{BL}+R_{BR}+R_{BG})]^{-1}$, MR is nearly completely absent. As V_A approaches $V_{depl} = -0.42$ V, however, a cusp in R_{SD} appears at ~ 1.3 T. As V_A is biased beyond V_{depl}, the size of the cusp remains relatively unchanged, while the entire R_{SD} curve is shifted upward, due to the depletion of QW1 beneath gate A. The B position of the cusp remains unchanged, as expected: the MR is nearly entirely due to the $R_{\text{tun}}(B)$'s.

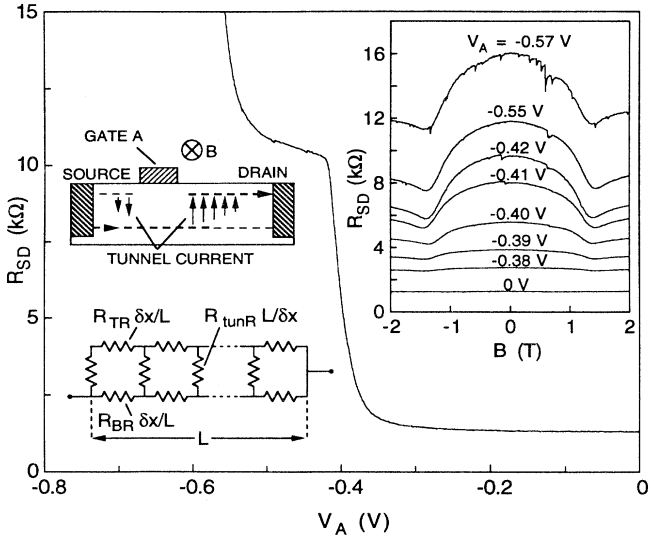

FIG. 2. R_{SD} as a function of V_A, at $V_B = 0$. The plateau at $V_A = -0.42$ V corresponds to the top well depletion. The upper-left inset depicts an idealized side view of the sample at $V_A = V_{depl}$, with arrows illustrating the current distribution. Most tunneling events occur to the right of the gate. The lower-left inset shows the transmission-line model used for the region of the sample to the right of gate A, with the differential resistance elements indicated. The right inset shows $R_{SD}(B)$ for several values of V_A, with $V_B = 0$.

We now turn in more detail to the magnetotunneling behavior. In Fig. 3(a) is shown $R_{SD}(B)$, after thermally cycling to 300 K, for $V_A = V_{depl}$. [The thermal cycling left V_{depl} unchanged, while $R_{SD}(B)$ and QW1 and QW2 resistivities decreased by about a factor of 2.] $R_{SD}(B)$ exhibits two sharp minima or cusps at $B \cong 1$ and 5.6 T. For $B \geq 9$ T, $R_{SD}(B)$ saturates at a value of ~ 4.9 kΩ. We can understand the MR cusps by applying the same dual-Fermi circle picture as before, modified for the $B \neq 0$ case by requiring the conservation of canonical momentum.[5–7] The momentum $\mathbf{p}$ in the Hamiltonian is replaced by the canonical momentum $\mathbf{p} + e\mathbf{A}$, where $\mathbf{A}$ is the magnetic-vector potential. With the QW's in the x-y plane and $\mathbf{B}$ in the y direction, we choose the Landau gauge so that $A_x = zB$, $A_y = A_z = 0$. Choosing $z = 0$ at QW1 thus causes the x-momentum term $\hbar k_x$ for QW2 to be replaced by $\hbar(k_x + edB/\hbar)$, where d is the center-to-center distance between the QW's, or 215 Å for our sample. Thus QW2's Fermi circle is displaced relative to QW1's by $\Delta k = edB/\hbar$. When the perimeters of the two Fermi circles overlap [see Fig. 3(a), insets], states of identical canonical momentum exist at the Fermi energy in both wells, and tunneling can occur. Tunneling is greatest at the tangential intersection points $\Delta k = k_1 - k_2$ and $k_1 + k_2$, where k_1 and k_2 are the Fermi wave numbers of QW1 and QW2. At high B, the Fermi circles completely separate, and tunneling is suppressed. This

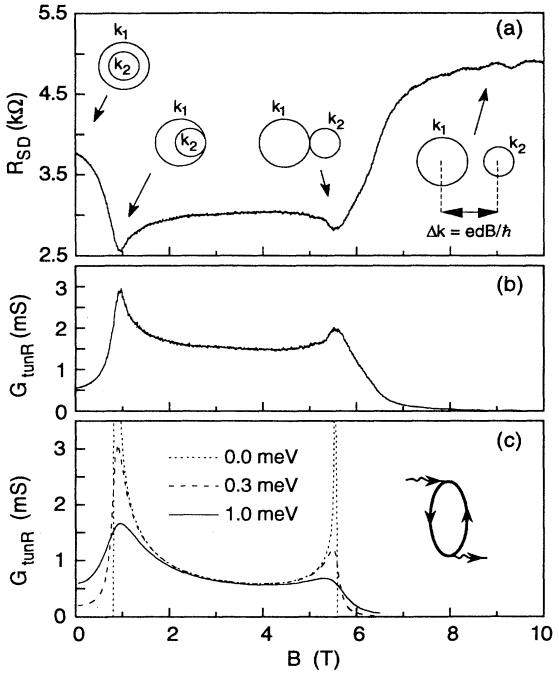

FIG. 3. (a) $R_{SD}(B)$ over the range 0–10 T. Insets depict top- and bottom-well Fermi circle positions for various regions of $R_{SD}(B)$. (b) G_{tunR} obtained from the data of (a) using Eq. (1). (c) Theoretical G_{tunR} from Eq. (2), for three values of Γ_1, at $T=0.3$ K. The inset shows a basic bubble diagram for the velocity-velocity correlation function in the tunneling conductivity.

provides a means of determining the R_B's and R_T's: $R_{BL}+R_{BR}+R_{BG}$ is given simply by the high-B saturation value of R_{SD}, when current travels only through QW1, with the three R_B's assumed to scale as their associated lengths. Similarly, given the R_B's, one can now find the R_T's (also assumed to scale as their lengths) from

$$R_{SD}(V_A=0)=[1/(R_{TL}+R_{TR}+R_{TG}) + 1/(R_{BL}+R_{BR}+R_{BG})]^{-1}$$

independent of B. Applying this method to the data of Fig. 3(a), for which $R_{SD}(V_A=0)=0.66$ kΩ, and assuming an effective gate width of 1 μm, from Eq. (1) we obtain $G_{tunR}(B)=1/R_{tunR}(B)$, which is plotted in Fig. 3(b).

It is desirable to include the effects of scattering here. In our structure, the tunneling integral is very small (~0.03 meV), and electrons suffer many scattering events before tunneling into the other well. The tunneling rate depends sensitively on the scattering rates in both the QW's, and even diverges at resonance for infinitely long scattering times within the Fermi golden rule approximation at $T=0$. Since it is not obvious how to correctly incorporate energy-level damping in a simple Fermi golden rule approach, we employ the more rigorous full field-theoretic Green's-function method and use Kubo's formalism.[10] The main contribution to the tunneling conductivity σ_{tun} arises from the basic "bubble" diagram depicted in the inset of Fig. 3(c), where the solid directed lines indicate dressed electron propagators in QW1 and QW2, and the wiggly directed lines represent the external-field vertices, signifying the tunneling velocity $v=J_k d/\hbar$. The tunneling conductivity is then given by

$$\sigma_{tun}=\frac{e^2d^2}{\Omega}\frac{4\pi}{\hbar}\sum_k J_k^2\int_{-\infty}^{\infty}d\xi[-f'(\xi)]L_{1k}(\xi)L_{2k}(\xi)\ , \tag{2}$$

where

$$L_{nk}(\xi)=\frac{\Gamma_{nk}}{\pi[(\xi-\varepsilon_{nk})^2+\Gamma_{nk}^2]}\quad (n=1,2)\ . \tag{3}$$

In Eq. (2), $\Omega=Sd$, where S is the tunneling area, J_k is the tunneling integral, and $f'(\xi)$ the first derivative of the Fermi function. In Eq. (3), Γ_{nk} represents the damping for state $\mathbf{k}$ in the nth QW and is related to the transport relaxation time by $\Gamma_{nk}^{iso}=\hbar\tau_{n,k}^{-1}/2$ for isotropic scattering. For anisotropic scattering, Γ_{nk} is larger than Γ_{nk}^{iso}. The wave vector $\mathbf{k}$ is independent of B in QW1, while in QW2 its x component is modified to $k_x(B)=k_x(0)+\Delta k$. The main effect of the finite well widths on the energy dispersion for ε_{nk} in an in-plane B is to modify the effective mass and introduce a nonparabolic term.[11] However, this effect is small for the B fields used here, and so is not included. Though Eq. (2) contains contributions from all sublevels, only the ground sublevels yield significant contributions at 0.3 K. Details will be published elsewhere.[12]

In the limit $\Gamma_2\ll\Gamma_1$, which is well satisfied in our structure, σ_{tun} becomes independent of Γ_2. In Fig. 3(c), we show $G_{tunR}(B)$ obtained from a numerical evaluation of Eq. (2) for $\Gamma_1=0.0$, 0.3, and 1.0 meV, which correspond to mobilities of ∞, 2.8×10^4, and 0.9×10^4 cm^2/V s for isotropic scattering. The other parameters used are $n_1=1.74\times10^{11}$ cm^{-2}, $n_2=0.95\times10^{11}$ cm^{-2}, $T=0.3$ K, $d=215$ Å, and a tunneling area of 20 μm^2 for the region to the right of gate B. The only adjustable parameter is the tunneling integral, for which we use 0.04 meV, larger than our actual estimate of 0.03 meV. The theory exhibits good qualitative agreement with the data in both magnitude and the half-widths of the tunneling peaks.

In order to further test our interpretation of the data, after again thermally cycling the sample we biased gate B positively while holding V_A at $V_{depl}=-0.45$ V (see Fig. 4). As V_B is increased, the top well density n_2 (and thus k_2) beneath gate B is increased, locally bringing the two wells closer to density balance. Thus for the regions under gate B, this (i) produces a shift in the peaks in σ_{tun} at the Fermi circle tangential intersection points $(k_1-k_2)\hbar/ed$ and $(k_1+k_2)\hbar/ed$; (ii) increases the size of the peaks in σ_{tun} by up to a factor of 2 since, as the curvatures of the Fermi circles approach one another, more states become available for tunneling; and (iii) changes the spatial distribution of the tunneling current, in part due to the shifted and enhanced peaks in σ_{tun} under gate B, and in part due to the increasing conductivity of QW2 under gate B. Thus the first MR cusp moves to lower B and the second MR cusp moves to higher B. The overall

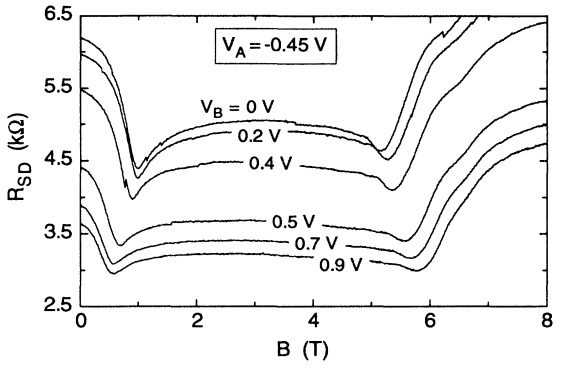

FIG. 4. $R_{SD}(B)$ for $V_A = V_{depl} = -0.45$ V, and several positive values of V_B.

decrease in R_{SD} is believed to be due at least in part to the increasing conductivity of QW2 (and, at high biases, QW1) under gate B. The data thus demonstrate control of 2D-2D tunneling on a scale of ≤ 1 μm, opening the possibility of producing quantum interference effects in similar structures.

At first glance one might expect the two MR cusps to *split* as V_B is increased, rather than just shift, since the sample regions far from gate B retain their original top well densities n_2'. However, the tunneling current in these regions is too small to produce MR cusps. We consider the three regions separately. (i) For the region between gates A and B, the distance between the gate edges is ~ 1.6 μm. Since at comparable densities depletion widths of up to ~ 1 μm have been observed,[13] and since a similar "enhancement width" is expected at the edge of gate B, this region is unlikely to contain a homogeneous domain of density n_2' of any consequential width, and thus will not produce sharp MR cusps. (ii) The region to the right of gate B, as borne out by extensive circuit simulations, carries negligible tunneling current, because the current path through QW1 has much higher resistance than that through QW2, *especially* when the peaks in σ_{tun} are enhanced under gate B. (iii) The region to the left of gate A is much shorter than that to the right. Because R_{BL} and R_{TL} scale directly with length, while R_{tunL} scales inversely, and because of the nonlinear behavior of the equivalent circuit, the tunneling current flowing in this region is nearly an order of magnitude lower than on the other side of gate A. When the peaks in σ_{tun} are enhanced under gate B, the ratio is even further decreased. Together, these factors reduce the strength of the original MR cusps to the point where they are unobservable.

In summary, we have examined interwell magnetotunneling in a double-QW heterostructure, utilizing a gated bridge technique which does not require independent contacts to the two 2D electron layers. The data agree with a linear-response theory based on a B-induced shift Δk of the wells' Fermi circles, and incorporating finite scattering times. A second gate is used to enhance tunneling locally on a length scale of ≤ 1 μm.

We thank T. Castillo for expert technical assistance. This work was supported by the U.S. DOE under Contract No. DE-AC04-76DP00789.

[1]For a review, see *The Physics of Quantum Electron Devices*, edited by F. Capasso, Springer Series in Electronics and Photonics Vol. 28 (Springer-Verlag, Berlin, 1990).
[2]R. A. Davies, D. J. Newson, T. G. Powell, M. J. Kelly, and H. W. Myron, Semicond. Sci. Technol. **2**, 61 (1987).
[3]M. L. Leadbeater, L. Eaves, P. E. Simmonds, G. A. Toombs, F. W. Sheard, P. A. Claxton, G. Hill, and M. A. Pate, Solid-State Electron. **31**, 707 (1988).
[4]P. England, J. R. Hayes, M. Helm, J. P. Harbison, L. T. Florez, and S. J. Allen, Jr., Appl. Phys. Lett. **54**, 1469 (1989).
[5]A. Zaslavsky, Yuan P. Li, D. C. Tsui, M. Santos, and M. Shayegan, Phys. Rev. B **42**, 1374 (1990).
[6]J. Smoliner, W. Demmerle, G. Berthold, E. Gornik, G. Weimann, and W. Schlapp, Phys. Rev. Lett. **63**, 2116 (1989).
[7]J. P. Eisenstein, T. J. Gramila, L. N. Pfeiffer, and K. W. West, Phys. Rev. B **44**, 6511 (1991).
[8]J. P. Eisenstein, L. N. Pfeiffer, and K. W. West, Appl. Phys. Lett. **58**, 1499 (1991).
[9]D. B. Scott, W. R. Hunter, and H. Shichijo, IEEE Trans. Electron Devices **ED-29**, 651 (1982).
[10]R. Kubo, J. Phys. Soc. Jpn. **12**, 570 (1957).
[11]S. K. Lyo and E. D. Jones, Solid State Commun. **83**, 975 (1992).
[12]S. K. Lyo and J. A. Simmons, J. Phys. C (to be published).
[13]K. K. Choi and D. C. Tsui, Appl. Phys. Lett. **50**, 110 (1987).